IEEE Access
Multidisciplinary | Rapid Review | Open Access Journal

Received September 30, 2017, accepted October 24, 2017, date of publication October 31, 2017,
date of current version November 28, 2017.

Digital Object Identifier 10.1109/ACCESS.2017.2768221

Joint 2D-DOA and Carrier Frequency Estimation Technique Using Nonlinear Kalman Filters for Cognitive Radio

SAMAR ELARABY[1], HEBA Y. SOLIMAN[1], (Member, IEEE), HEBA M. ABDEL-ATTY[1], (Member, IEEE), AND MOHAMED A. MOHAMED[2]

[1]Electrical Engineering Department, Faculty of Engineering, Port Said University, Port Said 42524, Egypt
[2]Electronics and Communication Engineering Department, Faculty of Engineering, Mansoura University, Mansoura 35516, Egypt

Corresponding author: Samar Elaraby (samar.elaraby@eng.psu.edu.eg)

ABSTRACT The problem of jointly estimating carrier frequencies and their corresponding two-dimension direction of arrivals (DOA) of band-limited source signals is considered in this paper for cognitive radio. The main problem of estimating carrier frequencies spread over a wideband spectrum is the requirement of high sampling rates. Thus, the Kalman filters are applied in the spatial domain instead of the temporal domain in the proposed algorithm to relax hardware complexity. The proposed algorithm exploits both the azimuth and elevation angles instead of a single DOA to increase the spatial capacity. Two approaches are proposed using two different types of nonlinear Kalman filter: extended Kalman filter (EKF) and unscented Kalman filter (UKF). Using simulations, the factors that affect the performance of both the filters are discussed. Scaling the estimated parameters to the same range and the proper tuning and initialization of the filters are crucial factors to prevent the filter divergence. Although UKF is supposed to have a better performance than EKF, reducing the inter-element spacing of the employed arrays and the proper filter initialization can make EKF approach the performance of UKF. On the other hand, UKF suffers from high processing time. Overall, both filters are able to converge to the true values of the unknown parameters using a number of relaxed analog-to-digital converters equal to the number of the array elements in the employed arrays. However, the approaches can detect a number of source signals higher than one-third of the total number of the array elements.

INDEX TERMS 2D-DOA estimation, cognitive radio, extended Kalman filter, spectrum sensing, unscented Kalman filter.

I. INTRODUCTION

Recently, the problem of radio frequencies shortage has grabbed the attention of researchers as radio devices have increased tremendously. In the next few years, radio applications and devices are expected to exponentially grow due to the growth of Internet of things (IoT) and machine to machine (M2M) communication. In IoT, millions of edges and radio devices are going to communicate on radio frequencies, however the existing spectrum is limited and cannot be expanded to embrace the rising demand. As a result, the opportunistic spectrum access has been suggested to solve the frequency band shortage. CR is one of the technologies that implement opportunistic spectrum access [1]. CR is a radio device that detects the frequency bands left unoccupied by their licensed users. This process is called spectrum sensing. Besides, while CR is transmitting on a particular frequency band, it continues to sense the spectrum to check for the presence of the licensed user and prevent the interference with it. This way, the spectrum can be exploited wisely and many CRs can share the limited resources. In the last decade, many proposals for spectrum sensing have been presented in the literature [2] and [3].

To increase the number of CRs that can share the unoccupied frequency bands in the same area, multiantenna techniques have been suggested to exploit the spatial domain. Then, CR can detect the presence of the licensed users and their transmitting directions. As a result, the spectral and spatial domains can be exploited efficiently. The main challenge facing the problem of estimating both spectral and spatial domains is the need to sample a wideband spectrum

at Nyquist rates. Nyquist rates require a high-speed ADC and generate a large number of samples to be processed. Thus, many proposals have been presented at sub-Nyquist sampling rates. In [4] and [5], the authors have proposed new architectures that can sample a wideband spectrum at sub-Nyquist rates with relaxed hardware requirements. Using ESPRIT [6] and MUSIC [7] algorithms, the authors have succeeded to estimate carrier frequencies and the corresponding DOAs. In [8], the authors have refined the estimated carrier frequencies and the corresponding DOAs using 2D-iterative grid refinement. In contrast, the authors in [9] have executed sub-Nyquist sampling using a modulated wideband converter (MWC) channel [10]. The authors have then proposed two algorithms to detect carrier frequencies and the corresponding DOAs. The first algorithm depends on compressive sensing, which was exploited to reconstruct the spectrum before estimating the desirable parameters. The second one is based on parallel factor (PARAFAC) analysis method [11]. A third algorithm, which depends on ESPRIT algorithm, has been proposed in [12].

The problem of these proposals is the limitation on the degrees of freedom; thus the number of detected sources is limited to the number of array elements. Increasing the degrees of freedom requires employing sparse antennas. So, the authors in [13] have employed a 2D nested array to raise the degrees of freedom. However, the proposal in [14] has increased the degrees of freedom using several MWCs at each element in the antenna. Since there is no need to reconstruct the whole spectrum to detect the existing carrier frequencies, the authors in [15] have decided to detect carrier frequencies and their corresponding DOAs from a reconstructed 2D power spectrum. The 2D angular power spectrum has been reconstructed from sub-Nyquist samples generated by multi-coset samplers. Besides, the authors have compressed the spatial measurements as well using a minimum redundancy linear array to increase the degrees of freedom.

Furthermore, a more efficient scenario has addressed the idea of investigating 2D-DOA instead of a single DOA, which represents a single direction around CR. Then, a CR can share the same carrier frequency and azimuth angle with a licensed user, but they differ in the elevation angles. This, in turn, increases the spatial capacity. The problem of jointly estimating 2D-DOA and carrier frequencies of primary users (PUs) has been discussed in the literature. ESPRIT algorithm is widely applied on this problem. In [16], the authors have relied on ESPRIT algorithm to detect carrier frequencies from sub-Nyquist samples of source signals that impinge on a uniform circular array. Then, 2D-DOA can be estimated. The authors in [17] have also implemented ESPRIT algorithm to estimate 2D-DOA using an L-shaped array. However, carrier frequencies have been estimated by singular value decomposition technique (SVD). In [18], ESPRIT algorithm has been extended to estimate both carrier frequencies and 2D-DOA. In [19], another ESPRIT-based algorithm has been proposed for estimating the carrier frequencies and their corresponding 2D-DOA of multi-band signals from the outputs of a uniform rectangular array (URA). Moreover, the PARAFAC analysis has been proposed for carrier frequency and 2D-DOA estimation with a conformal array in [20] and [21]. In [22], the authors have proposed iterative least square methods for both frequency and 2D-DOA estimation problem.

In this paper, the problem of jointly estimating the carrier frequencies and their corresponding azimuth and elevation angles of uncorrelated band-limited source signals is considered. To the best of our knowledge, Kalman filter (KF) has not been exploited in this problem before. KF is a recursive algorithm that can estimate unknown parameters from a state space model with noisy measurements [23], and the state space model can be formulated in any domain. Since the considered problem has to tackle the sampling of a wideband spectrum, we propose investigating the spatial domain using KF instead of relying on sub-Nyquist methods in the temporal domain. Two L-shaped uniform arrays are employed in our proposal to form the spatial state space model that KF would follow to predict the desired unknown parameters. Thus, one time sample at each array element is only required to identify the time delay encountered by any source signal between any two successive array elements. As a result, our proposal does not have to sample a wideband spectrum at Nyquist or sub-Nyquist rates leading to gaining an advantage over the other methods in the literature in terms of hardware complexity. In other words, there are not any restrictions on the sampling rate, and hence the speed of the employed ADCs has no restrictions as well. Furthermore, the required number of the relaxed ADCs by sub-Nyquist methods is reduced to the number of the employed array elements. On the other hand, since our proposal relies on a uniform dense array, it has limited degrees of freedom. The degrees of freedom are found to be equal to one third of the employed array elements. To implement our proposal, we have exploited two different types of nonlinear Kalman filters, extended Kalman filter (EKF) [23] and unscented Kalman filter (UKF) [24]. Since nonlinear KFs are sub-optimal estimators, they may tend to converge to wrong values or even completely diverge. The performance of the two algorithms is examined under different conditions using simulations, and the factors that can affect their performance are discussed.

The paper is organized as follows. Section II describes the two L-shaped array model. Kalman filter and its different types are then visited in Section III. Section IV declares a detailed analysis of our proposal. Proposed spatial state space model is first derived. Then, a detailed description of both EKF-based and UKF-based approaches is presented. Simulations with discussions are addressed in Section V. Finally, Section VI derives final conclusions.

II. SYSTEM MODEL

Consider two L-shaped uniform arrays located in the x-z plane and the y-z plane as shown in Figure 1. Each single uniform linear array (ULA) in this structure has N elements with an inter-element spacing of d. The element at the origin is considered as a reference point. Suppose that L different

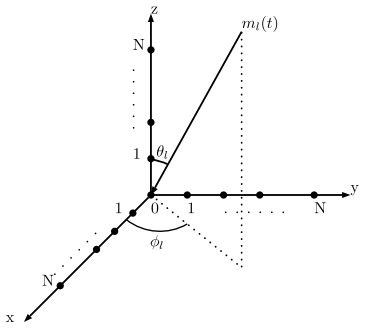

FIGURE 1. Two L-shaped uniform array model.

band-limited signals from L different uncorrelated sources are impinging on the two L-shaped arrays. Each source signal is transmitted from a different direction on a different carrier frequency. Then, the output of each element can be evaluated as

$$\begin{aligned} r_x^n(t) &= \sum_{l=1}^{L} m_l(t) e^{-j2\pi(n-1)d\frac{\cos\phi_l \sin\theta_l}{\lambda_l}} + \eta_x^n(t) \\ r_y^n(t) &= \sum_{l=1}^{L} m_l(t) e^{-j2\pi(n-1)d\frac{\sin\phi_l \sin\theta_l}{\lambda_l}} + \eta_y^n(t) \\ r_z^n(t) &= \sum_{l=1}^{L} m_l(t) e^{-j2\pi(n-1)d\frac{\cos\theta_l}{\lambda_l}} + \eta_z^n(t) \end{aligned} \quad (1)$$

where $r_x^n(t)$, $r_y^n(t)$ and $r_z^n(t)$ are the outputs of the n^{th} element in the ULA located on x-axis, y-axis and z-axis respectively. The signal $m_l(t)$, with $l = 1, 2 \ldots L$, denotes the received source signal at the reference point from the l^{th} source. The signal $m_l(t)$ has a wavelength of λ_l and arrives from a direction with an azimuth angle of ϕ_l and an elevation angle of θ_l. Noise signals $\eta_x^n(t)$, $\eta_y^n(t)$ and $\eta_z^n(t)$ are assumed to be complex Gaussian white noise with zero mean and variance of σ_n^2.

Since CRs are not allowed to have any prior information about licensed users being detected, the problem considered in this paper is a blind estimation problem. The CR has to blindly estimate the carrier frequency and the corresponding 2D-DOA of the surrounding licensed users. For this problem, we propose Kalman filter for estimating λ_l, ϕ_l and θ_l of each licensed user.

III. KALMAN FILTERS: AN OVERVIEW

KF is an algorithm that optimally estimates an unknown state variable from a state space model based on noisy measurements. First, KF algorithm predicts the posterior estimate of the state variable from the previous estimate. Then, the predictions are adjusted according to observed measurements. The two steps are repeated till the filter converges to the true estimate of the state variable. KF is an optimal algorithm as it depends on linear state space models. A linear state space model can be generally described as a combination of process space model and measurement space model as follows

$$\begin{aligned} \mathbf{x}_{n+1} &= \mathbf{A}\mathbf{x}_n + \mathbf{w}_n \\ \mathbf{Y}_n &= \mathbf{H}\mathbf{x}_n + \mathbf{u}_n \end{aligned} \quad (2)$$

where $\mathbf{x}_{n+1}$ and $\mathbf{x}_n$ denote posterior and prior estimate of the state variable respectively. Matrices $\mathbf{A}$ and $\mathbf{H}$ represent transition matrix and observation matrix respectively. However, $\mathbf{w}_n$ and $\mathbf{u}_n$ respectively denote process noise and measurements noise signals, which are assumed to be Gaussian distributed with zero mean and covariance matrix of $\mathbf{Q}$ and $\mathbf{R}$ respectively. The process noise covariance matrix $\mathbf{Q}$ represents uncertainty in process space model. However, the measurement noise covariance matrix $\mathbf{R}$ represents uncertainty in observed measurements. While KF estimates the state variable, it can estimate unknown parameters as well. As a result, it is used intensively in estimation problems where the unknown parameters are concatenated to the state variable. Then, they can be estimated with it through iterations.

In many estimation problems, the state space model may have a nonlinear process model and/or a nonlinear measurement model. The nonlinear state space model has the form of

$$\begin{aligned} \mathbf{x}_{n+1} &= f(\mathbf{x}_n) + \mathbf{w}_n \\ \mathbf{Y}_n &= h(\mathbf{x}_n) + \mathbf{u}_n \end{aligned} \quad (3)$$

where $f(.)$ and $h(.)$ represent nonlinearity in the process and measurement models respectively. For nonlinear state space models, traditional KF fails to converge to the true values and modifications to KF are required resulting in sub-optimal performance. Two of the renowned nonlinear KFs are EKF and UKF.

In EKF, nonlinear models are linearized about the estimated trajectory. It relies on Taylor series to execute linearization and the resultant is approximated to the first order derivatives. The detailed EKF algorithm can be found in [23]. The linearization process results in significant errors in the estimated state variable and these errors are accumulated through iterations. On the other hand, the filter updates the estimated state variable each iteration based on noisy measurements. This, in turn, leads the estimated trajectory to follow the noisy measurements. As a result, the filter may converge to erroneous values or even completely diverge. To enhance the performance of EKF, the filter should be tuned and initialized properly. Tuning the filter means to choose a proper estimate for $\mathbf{Q}$ and $\mathbf{R}$ matrices to wisely build confidence in both process and measurement models respectively. Furthermore, we propose wisely choosing the parameters to be concatenated to the state variable instead of directly choosing carrier frequencies, azimuth angles and elevation angles themselves. In other words, the filter may converge to true estimates and its performance approaches the performance of traditional KF, if the unknown parameters are scaled to the same range with a small variance relative to a region where the model is relatively linear. In this range, linearization errors can be reduced and the filter performance can be enhanced. Simulations are presented to prove the vital role of the proper initialization in enhancing the filter performance.

In UKF, Gaussian-distributed state variable is captured by a minimal set of sample points, called sigma points.

These points are actually capturing both the mean and the variance of the state variable. After sigma points are propagated through the nonlinear filter, their outputs can be used to perfectly recover the estimated Gaussian state variable. In each iteration, the posterior estimates and covariance matrix are evaluated as weighted mean and covariance of the sigma point outputs. Through iterations, the filter tends to converge to the true values of the state variable. UKF, like EKF, needs to be properly tuned and initialized to enhance the filter convergence. The complete algorithm of UKF is proposed in [24]. In comparison to EKF, UKF is accurate to the third order derivative. Besides, UKF, unlike EKF, does not rely on evaluating partial derivatives. However, the complexity of UKF is higher than the complexity of EKF as UKF needs to calculate sigma points in each iteration.

IV. PROPOSED APPROACHES

In this section, we first derive the spatial state space from Eq. (1). Then, the proposed EKF-based and UKF-based approaches are presented in detail.

A. PROPOSED SPATIAL STATE SPACE

The main challenge of wideband spectrum sensing is to sample the signals at high Nyquist sampling rates, which require sophisticated high-speed ADCs. Since the array geometry provides an opportunity to exploit the spatial domain, we propose forming a spatial state space instead of a temporal state space to reduce the complexity associated with the latter. The spatial state space is formed from the time delay that each source signal encounters between any two successive array elements. The time delay is expressed as a phase shift between the different versions of the source signals arrive the elements. Therefore, the l^{th} source signal that reaches the $(n+1)^{th}$ element in the three different ULAs X_l^{n+1}, Y_l^{n+1} and Z_l^{n+1} can be determined as

$$\begin{aligned} X_l^{n+1} &= e^{-j2\pi d \frac{\cos\phi_l \sin\theta_l}{\lambda_l}} X_l^n \\ Y_l^{n+1} &= e^{-j2\pi d \frac{\sin\phi_l \sin\theta_l}{\lambda_l}} Y_l^n \\ Z_l^{n+1} &= e^{-j2\pi d \frac{\cos\theta_l}{\lambda_l}} Z_l^n \end{aligned} \tag{4}$$

where X_l^n, Y_l^n and Z_l^n are the versions of the l^{th} source signal reaches the n^{th} element. In matrix notation, Eq. (4) can be reformulated as follows

$$\begin{bmatrix} x_{2l-1}^{n+1} \\ x_{2l}^{n+1} \end{bmatrix} = \begin{bmatrix} \cos\left(2\pi d \frac{\cos\phi_l \sin\theta_l}{\lambda_l}\right) & \sin\left(2\pi d \frac{\cos\phi_l \sin\theta_l}{\lambda_l}\right) \\ -\sin\left(2\pi d \frac{\cos\phi_l \sin\theta_l}{\lambda_l}\right) & \cos\left(2\pi d \frac{\cos\phi_l \sin\theta_l}{\lambda_l}\right) \end{bmatrix} \times \begin{bmatrix} x_{2l-1}^n \\ x_{2l}^n \end{bmatrix} \tag{5}$$

where x_{2l-1}^{n+1} and x_{2l}^{n+1} represent real and imaginary parts of X_l^{n+1}. Similarly,

$$\begin{bmatrix} y_{2l-1}^{n+1} \\ y_{2l}^{n+1} \end{bmatrix} = \begin{bmatrix} \cos\left(2\pi d \frac{\sin\phi_l \sin\theta_l}{\lambda_l}\right) & \sin\left(2\pi d \frac{\sin\phi_l \sin\theta_l}{\lambda_l}\right) \\ -\sin\left(2\pi d \frac{\sin\phi_l \sin\theta_l}{\lambda_l}\right) & \cos\left(2\pi d \frac{\sin\phi_l \sin\theta_l}{\lambda_l}\right) \end{bmatrix} \times \begin{bmatrix} y_{2l-1}^n \\ y_{2l}^n \end{bmatrix} \tag{6}$$

and

$$\begin{bmatrix} z_{2l-1}^{n+1} \\ z_{2l}^{n+1} \end{bmatrix} = \begin{bmatrix} \cos\left(2\pi d \frac{\cos\theta_l}{\lambda_l}\right) & \sin\left(2\pi d \frac{\cos\theta_l}{\lambda_l}\right) \\ -\sin\left(2\pi d \frac{\cos\theta_l}{\lambda_l}\right) & \cos\left(2\pi d \frac{\cos\theta_l}{\lambda_l}\right) \end{bmatrix} \times \begin{bmatrix} z_{2l-1}^n \\ z_{2l}^n \end{bmatrix} \tag{7}$$

The state variable $\mathbf{x}_s \in \mathbb{R}^{6L\times 1}$ is then formed at any element as a concatenation of the real and imaginary values in the three ULAs as follows

$$\mathbf{x}_s = [x_1,\ x_2 \ldots x_{2L-1},\ x_{2L},\ y_1,\ y_2\ \ldots\ y_{2L-1},\ y_{2L},\ z_1,\ z_2,\ \ldots\ z_{2L-1},\ z_{2L}]^T \tag{8}$$

Since Kalman filters are considered to predict unknown parameters, these parameters should be concatenated to the state variable. Then in each iteration of the kalman filtering, the parameters are estimated as well as the posterior estimate of the state variable. The parameters to be estimated in our problem are carrier frequency, azimuth and elevation angles of the L sources. These parameters are not going to be concatenated to the state variable directly as they vary over different wide ranges and may force EKF to diverge. So, we propose selecting related parameters that share the same range to speed up the filter convergence and boost the filter performance. The parameters are selected to be

$$\begin{aligned} a_l &= \frac{\cos\phi_l \sin\theta_l}{\lambda_l}, \quad b_l = \frac{\sin\phi_l \sin\theta_l}{\lambda_l} \\ c_l &= \frac{\cos\theta_l}{\lambda_l} \end{aligned} \tag{9}$$

where $l = 1, 2 \ldots L$. By estimating these parameters using Kalman filter, ϕ_l, θ_l and λ_l can be evaluated for each source. Moreover, the inter-element spacing d is set to a fraction of the minimum wavelength. Reducing d as possible can result in expanding the sinusoidal model in Eq. (5) - (7) regarding to the unknown parameters. This, in turn, leads the filter to search through a region where the model is relatively linear. Under this scenario, both EKF and UKF can overcome their sub-optimal performance and converge to more precise values. Using simulation in Section V, an enhanced performance is proven while decreasing d.

Now, the state variable becomes $\mathbf{x}_s \in \mathbb{R}^{9L\times 1}$ and the process model of the spatial state space model can be defined

$$\mathbf{x}_s^{n+1} = \begin{bmatrix} \boldsymbol{\alpha}_x & 0 & 0 & 0 & 0 & 0 \\ 0 & \boldsymbol{\alpha}_y & 0 & 0 & 0 & 0 \\ 0 & 0 & \boldsymbol{\alpha}_z & 0 & 0 & 0 \\ 0 & 0 & 0 & \mathbf{I} & 0 & 0 \\ 0 & 0 & 0 & 0 & \mathbf{I} & 0 \\ 0 & 0 & 0 & 0 & 0 & \mathbf{I} \end{bmatrix} \mathbf{x}_s^n \tag{10}$$

where $\mathbf{I} \in \mathbb{R}^{L\times L}$ is the identity matrix. The submatrices $\boldsymbol{\alpha}_x$, $\boldsymbol{\alpha}_y$ and $\boldsymbol{\alpha}_z \in \mathbb{R}^{2L\times 2L}$ are defined as

$$\boldsymbol{\alpha}_x = \begin{bmatrix} \boldsymbol{\alpha}_{x1} & 0 & 0 \\ 0 & \ddots & 0 \\ 0 & 0 & \boldsymbol{\alpha}_{xL} \end{bmatrix}, \quad \boldsymbol{\alpha}_y = \begin{bmatrix} \boldsymbol{\alpha}_{y1} & 0 & 0 \\ 0 & \ddots & 0 \\ 0 & 0 & \boldsymbol{\alpha}_{yL} \end{bmatrix},$$
$$\boldsymbol{\alpha}_z = \begin{bmatrix} \boldsymbol{\alpha}_{z1} & 0 & 0 \\ 0 & \ddots & 0 \\ 0 & 0 & \boldsymbol{\alpha}_{zL} \end{bmatrix} \tag{11}$$

where

$$\boldsymbol{\alpha}_{xl} = \begin{bmatrix} \cos\left(2\pi d \frac{\cos\phi_l \sin\theta_l}{\lambda_l}\right) & \sin\left(2\pi d \frac{\cos\phi_l \sin\theta_l}{\lambda_l}\right) \\ -\sin\left(2\pi d \frac{\cos\phi_l \sin\theta_l}{\lambda_l}\right) & \cos\left(2\pi d \frac{\cos\phi_l \sin\theta_l}{\lambda_l}\right) \end{bmatrix}$$
$$\boldsymbol{\alpha}_{yl} = \begin{bmatrix} \cos\left(2\pi d \frac{\sin\phi_l \sin\theta_l}{\lambda_l}\right) & \sin\left(2\pi d \frac{\sin\phi_l \sin\theta_l}{\lambda_l}\right) \\ -\sin\left(2\pi d \frac{\sin\phi_l \sin\theta_l}{\lambda_l}\right) & \cos\left(2\pi d \frac{\sin\phi_l \sin\theta_l}{\lambda_l}\right) \end{bmatrix}$$
$$\boldsymbol{\alpha}_{zl} = \begin{bmatrix} \cos\left(2\pi d \frac{\cos\theta_l}{\lambda_l}\right) & \sin\left(2\pi d \frac{\cos\theta_l}{\lambda_l}\right) \\ -\sin\left(2\pi d \frac{\cos\theta_l}{\lambda_l}\right) & \cos\left(2\pi d \frac{\cos\theta_l}{\lambda_l}\right) \end{bmatrix} \tag{12}$$

with $l = 1, 2, \ldots L$.

However, the measurement model of the spatial state space represents the measured output at the n^{th} element in all arrays. The measured output at the n^{th} element is expected to be the sum of all incident source signals on this element. It is, however, exposed to measurement errors and hence the measurement model can be declared in matrix notation as

$$\mathbf{Y}_n = [Y^n_{x,re}\ Y^n_{x,im}\ Y^n_{y,re}\ Y^n_{y,im}\ Y^n_{z,re}\ Y^n_{z,im}]^T = \begin{bmatrix} 1 & 0 & & 0 & 0 & & 0 & 0 & 0 & & 0 \\ 0 & 1 & & 0 & 0 & & 0 & 0 & 0 & & 0 \\ 0 & 0 & \ldots & 1 & 0 & \ldots & 0 & 0 & 0 & \ldots & 0 \\ 0 & 0 & & 0 & 1 & & 0 & 0 & 0 & & 0 \\ 0 & 0 & & 0 & 0 & & 1 & 0 & 0 & & 0 \\ 0 & 0 & & 0 & 0 & & 0 & 1 & 0 & & 0 \end{bmatrix} \mathbf{x}_s^n + \mathbf{u}_n \tag{13}$$

where $Y^n_{x,re}$, $Y^n_{y,re}$ and $Y^n_{z,re}$ are the real parts of the n^{th} element outputs in the x-array, y-array and z-array respectively. The remaining terms $Y^n_{x,im}$, $Y^n_{y,im}$ and $Y^n_{z,im}$ are the imaginary parts of these outputs respectively. The vector $\mathbf{u}_n$ represents the measurement noise signals which has zero-mean and covariance matrix $\mathbf{R}$.

The spatial state model is now formulated and it obviously contains a nonlinear process model as in Eq. (3) and a linear measurement model as in Eq. (2). Thus, sub-optimal EKF and UKF are proposed for the nonlinearity of this problem. While applying these filters to the proposed state model, the process noise covariance matrix $\mathbf{Q}$ is set to zero giving full trust in the proposed process model.

B. PROPOSED EXTENDED KALMAN FILTER-BASED APPROACH

In the first approach, we propose EKF algorithm, described in [23], for estimating the state variable $\mathbf{x}_s$ from the formulated state space model. First, EKF is initialized with an initial estimate $\hat{\mathbf{x}}_0$ and initial covariance matrix $\mathbf{P}_0$. The initial estimate $\hat{\mathbf{x}}_0$ is preferable to be selected close to the mean value of the state variable to speed up the convergence to the true values. Moreover, the matrix $\mathbf{P}_0$ should be carefully selected as it may be set to a low value that is enough to force the filter to fully trust the posterior estimates and neglect the effect of measurements.

Then, EKF goes through several iterations and each iteration consists of two steps: prediction step that follows the process model and updating step that follows the measurement model as shown in Algorithm 1. In each prediction step, the nonlinear process model must be linearized around the

Algorithm 1 EKF-Based Proposed Algorithm

0: Intialization:

$$\hat{\mathbf{x}}_0 = \mathrm{E}[\mathbf{x}_s]$$
$$\mathbf{P}_0 = \mathrm{E}[(\mathbf{x}_s - \hat{\mathbf{x}}_0)(\mathbf{x}_s - \hat{\mathbf{x}}_0)^T]$$

1: loop

Prediction Step:

$$\mathbf{F}_n = \frac{\partial f(\mathbf{x}_s^{n-1})}{\partial \mathbf{x}_s^{n-1}}\Big|_{\mathbf{x}_s^{n-1}=\hat{\mathbf{x}}_{n-1}}$$
$$\hat{\mathbf{x}}_n^- = f(\hat{\mathbf{x}}_{n-1})$$
$$\mathbf{P}_n^- = \mathbf{F}_n \mathbf{P}_{n-1} \mathbf{F}_n^T$$

Updating Step:

$$\mathbf{K}_n = \mathbf{P}_n^- \mathbf{H}^T (\mathbf{R} + \mathbf{H}\mathbf{P}_n^- \mathbf{H}^T)^{-1}$$
$$\hat{\mathbf{x}}_n = \hat{\mathbf{x}}_n^- + \mathbf{K}_n (\mathbf{Y}_n - \mathbf{H}\hat{\mathbf{x}}_n^-)$$
$$\mathbf{P}_n = \mathbf{P}_n^- - \mathbf{K}_n \mathbf{H} \mathbf{P}_n^-$$

if convergence:

for each source:

$$\phi_l = \tan^{-1}\left(\frac{b_l}{a_l}\right)$$
$$\theta_l = \tan^{-1}\left(\frac{b_l}{c_l}\right)$$
$$\lambda_l = \frac{\cos\theta_l}{c_l}$$

break loop

prior estimates. Then, the approximated resultant to the first order derivatives is calculated as a Jacobian matrix $\mathbf{F}_n$

$$\mathbf{F}_n = \frac{\partial f(\mathbf{x}_s^{n-1})}{\partial \mathbf{x}_s^{n-1}}\Big|_{\mathbf{x}_s^{n-1}=\hat{\mathbf{x}}_{n-1}} = \begin{bmatrix} \mathbf{f}_1 & 0 & 0 & \mathbf{f}_4 & 0 & 0 \\ 0 & \mathbf{f}_2 & 0 & 0 & \mathbf{f}_5 & 0 \\ 0 & 0 & \mathbf{f}_3 & 0 & 0 & \mathbf{f}_6 \\ 0 & 0 & 0 & \mathbf{I} & 0 & 0 \\ 0 & 0 & 0 & 0 & \mathbf{I} & 0 \\ 0 & 0 & 0 & 0 & 0 & \mathbf{I} \end{bmatrix} \tag{14}$$

where $\mathbf{I} \in \mathbb{R}^{L\times L}$ is the identity matrix. The matrices $\mathbf{f}_1, \mathbf{f}_2, \mathbf{f}_3, \mathbf{f}_4, \mathbf{f}_5$ and $\mathbf{f}_6$ are defined as follows

$$\mathbf{f}_1 = \begin{bmatrix} \ddots & 0 & 0 \\ 0 & \boldsymbol{\beta}_{1l} & 0 \\ 0 & 0 & \ddots \end{bmatrix}, \quad l = 1, 2, \ldots L \tag{15}$$

where

$$\begin{aligned} \boldsymbol{\beta}_{1l} &= \begin{bmatrix} \frac{\partial x_{2l-1}^n}{\partial x_{2l-1}^{n-1}} & \frac{\partial x_{2l-1}^n}{\partial x_{2l}^{n-1}} \\ \frac{\partial x_{2l}^n}{\partial x_{2l-1}^{n-1}} & \frac{\partial x_{2l}^n}{\partial x_{2l}^{n-1}} \end{bmatrix}_{\mathbf{x}_s^{n-1}=\hat{\mathbf{x}}_{n-1}} \\ &= \begin{bmatrix} \cos\left(2\pi d\hat{a}_l^{n-1}\right) & \sin\left(2\pi d\hat{a}_l^{n-1}\right) \\ -\sin\left(2\pi d\hat{a}_l^{n-1}\right) & \cos\left(2\pi d\hat{a}_l^{n-1}\right) \end{bmatrix} \end{aligned} \tag{16}$$

Similarly, the remaining matrices $\mathbf{f}_2, \mathbf{f}_3, \mathbf{f}_4, \mathbf{f}_5$ and $\mathbf{f}_6$ are diagonal and their diagonals have the elements $\boldsymbol{\beta}_{2l}, \boldsymbol{\beta}_{3l}, \boldsymbol{\beta}_{4l}, \boldsymbol{\beta}_{5l}$ and $\boldsymbol{\beta}_{6l}$ respectively. In the same manner, they are evaluated as

$$\begin{aligned} \boldsymbol{\beta}_{2l} &= \begin{bmatrix} \cos\left(2\pi d\hat{b}_l^{n-1}\right) & \sin\left(2\pi d\hat{b}_l^{n-1}\right) \\ -\sin\left(2\pi d\hat{b}_l^{n-1}\right) & \cos\left(2\pi d\hat{b}_l^{n-1}\right) \end{bmatrix} \\ \boldsymbol{\beta}_{3l} &= \begin{bmatrix} \cos\left(2\pi d\hat{c}_l^{n-1}\right) & \sin\left(2\pi d\hat{c}_l^{n-1}\right) \\ -\sin\left(2\pi d\hat{c}_l^{n-1}\right) & \cos\left(2\pi d\hat{c}_l^{n-1}\right) \end{bmatrix} \\ \boldsymbol{\beta}_{4l} &= 2\pi d \begin{bmatrix} -\sin\left(2\pi d\hat{a}_l^{n-1}\right) & \cos\left(2\pi d\hat{a}_l^{n-1}\right) \\ -\cos\left(2\pi d\hat{a}_l^{n-1}\right) & -\sin\left(2\pi d\hat{a}_l^{n-1}\right) \end{bmatrix} \\ &\quad \times \begin{bmatrix} \hat{x}_{2l-1}^{n-1} \\ \hat{x}_{2l}^{n-1} \end{bmatrix} \\ \boldsymbol{\beta}_{5l} &= 2\pi d \begin{bmatrix} -\sin\left(2\pi d\hat{b}_l^{n-1}\right) & \cos\left(2\pi d\hat{b}_l^{n-1}\right) \\ -\cos\left(2\pi d\hat{b}_l^{n-1}\right) & -\sin\left(2\pi d\hat{b}_l^{n-1}\right) \end{bmatrix} \\ &\quad \times \begin{bmatrix} \hat{y}_{2l-1}^{n-1} \\ \hat{y}_{2l}^{n-1} \end{bmatrix} \\ \boldsymbol{\beta}_{6l} &= 2\pi d \begin{bmatrix} -\sin\left(2\pi d\hat{c}_l^{n-1}\right) & \cos\left(2\pi d\hat{c}_l^{n-1}\right) \\ -\cos\left(2\pi d\hat{c}_l^{n-1}\right) & -\sin\left(2\pi d\hat{c}_l^{n-1}\right) \end{bmatrix} \\ &\quad \times \begin{bmatrix} \hat{z}_{2l-1}^{n-1} \\ \hat{z}_{2l}^{n-1} \end{bmatrix} \end{aligned} \tag{17}$$

After performing linearization by evaluating Jacobian matrix $\mathbf{F}_n$, the posterior estimate $\hat{\mathbf{x}}_n^-$ and covariance matrix $\mathbf{P}_n^-$ are predicted from their prior values $\hat{\mathbf{x}}_{n-1}$ and $\mathbf{P}_{n-1}$ respectively. The predicted estimates are then updated depending on the filter gain $\mathbf{K}_n$ and observation matrix $\mathbf{H}$ as shown in Algorithm 1. The filter then goes through several iterations of prediction and updating, till it finally tends to converge. The filter converges to the true values of a_l, b_l and c_l since the estimated parameters have a small variance compared to a region where the model is relatively linear. This, in turn, forces EKF to approach the performance of traditional linear KF. The unknown carrier frequencies and 2D-DOA angles are finally calculated from the estimated a_l, b_l and c_l.

C. PROPOSED UNSCENTED KALMAN FILTER-BASED APPROACH

The second approach proposes UKF algorithm, described in [24], for the considered estimation problem. The complete algorithm is described in Algorithm 2. First, the initial estimate $\hat{\mathbf{x}}_0^a$ and covariance matrix $\mathbf{P}_0^a$ are initialized properly. The initial estimate $\hat{\mathbf{x}}_0^a$ is a concatenation of the initial estimate of the state variable $\hat{\mathbf{x}}_0$ and the initial estimate of measurement noise. This, in turn, leads the initial covariance matrix $\mathbf{P}_0^a$ to gather both the covariance matrix of the state variable $\mathbf{P}_0 = \mathrm{E}[(\mathbf{x}_s - \hat{\mathbf{x}}_0)(\mathbf{x}_s - \hat{\mathbf{x}}_0)^T]$ and the measurement noise covariance matrix $\mathbf{P}_\upsilon$ (equivalent to $\mathbf{R}$ in EKF).

Then, the filter rotates in several iterations till the filter converges to the true values. In each iteration, sigma points $\boldsymbol{\chi}_{i,n-1}^a$, with $i = 0, 1 \ldots 18L$, are selected to perfectly capture the mean and variance of the state variable. Since a state variable of dimension M needs 2M+1 sigma points, the state variable $\mathbf{x}_s$ needs 18L+1 sigma points. These sigma points are evaluated as shown in Algorithm 2 by determining the i^{th} row of $\left(\sqrt{(6L+\Lambda)\mathbf{P}_{n-1}}\right)_i$ using Cholesky decomposition. The parameter Λ is a scaling parameter which equals to $\alpha^2(6L+\kappa) - 6L$ where α denotes the spread of sigma points around $\hat{\mathbf{x}}_n$ and κ is a secondary scaling parameter (usually equals to 0).

After selecting the sigma points, the filter executes prediction step in which the sigma points are propagated through the nonlinear process model, and the resultant is used to predict the posterior estimate $\hat{\mathbf{x}}_n^-$. The posterior estimate $\hat{\mathbf{x}}_n^-$ and covariance matrix $\mathbf{P}_n^-$ are evaluated as weighted mean and covariance matrix of the resultant. The employed weights are defines as

$$\begin{aligned} w_0^{(m)} &= \frac{\Lambda}{6L+\Lambda} \\ w_0^{(c)} &= \frac{\Lambda}{6L+\Lambda} + (1 - \alpha^2 + \beta) \\ w_i^{(m)} &= w_i^{(c)} = \frac{1}{2(6L+\Lambda)} \quad i = 1, 2, \ldots 18L \end{aligned} \tag{18}$$

where β represents the state variable distribution ($\beta = 2$ for Gaussian distribution).

Then, the filter executes updating step where the posterior estimate and covariance matrix are corrected by

Algorithm 2 UKF-Based Proposed Algorithm

0: Intialization:

$$\hat{\mathbf{x}}_0^a = [\hat{\mathbf{x}}_0^T \;\; 0]^T$$
$$\mathbf{P}_0^a = \begin{bmatrix} \mathbf{P}_0 & 0 \\ 0 & \mathbf{P}_\upsilon \end{bmatrix}$$

1: loop

Selecting Sigma Points:

$$\boldsymbol{\chi}_{0,n-1}^a = \hat{\mathbf{x}}_{n-1}^a$$
$$\boldsymbol{\chi}_{i,n-1}^a = \hat{\mathbf{x}}_{n-1}^a + \left(\sqrt{(6L+\Lambda)\mathbf{P}_{n-1}}\right)_i \quad i = 1, 2 \ldots 6L$$
$$\boldsymbol{\chi}_{i,n-1}^a = \hat{\mathbf{x}}_{n-1}^a - \left(\sqrt{(6L+\Lambda)\mathbf{P}_{n-1}}\right)_i \quad i = 6L+1, \ldots 12L$$

Prediction Step:

$$\boldsymbol{\chi}_{i,n|n-1}^x = f(\boldsymbol{\chi}_{i,n-1}^x)$$
$$\hat{\mathbf{x}}_n^- = \sum_{i=0}^{12L} w_i^{(m)} \, \boldsymbol{\chi}_{i,n|n-1}^x$$
$$\mathbf{P}_n^- = \sum_{i=0}^{12L} w_i^{(c)} \left(\boldsymbol{\chi}_{i,n|n-1}^x - \hat{\mathbf{x}}_n^-\right)\left(\boldsymbol{\chi}_{i,n|n-1}^x - \hat{\mathbf{x}}_n^-\right)^T$$

Updating Step:

$$\boldsymbol{\Psi}_{i,n|n-1} = \mathbf{H}\,\boldsymbol{\chi}_{i,n|n-1}^x + \boldsymbol{\chi}_{i,n|n-1}^n$$
$$\hat{\mathbf{y}}_n^- = \sum_{i=0}^{12L} w_i^{(m)} \, \boldsymbol{\Psi}_{i,n|n-1}$$
$$\mathbf{P}_{\tilde{y}_n\tilde{y}_n} = \sum_{i=0}^{12L} w_i^{(c)} \left(\boldsymbol{\Psi}_{i,n|n-1} - \hat{\mathbf{y}}_n^-\right)\left(\boldsymbol{\Psi}_{i,n|n-1} - \hat{\mathbf{y}}_n^-\right)^T$$
$$\mathbf{P}_{\tilde{x}_n\tilde{y}_n} = \sum_{i=0}^{12L} w_i^{(c)} \left(\boldsymbol{\chi}_{i,n|n-1}^x - \hat{\mathbf{x}}_n^-\right)\left(\boldsymbol{\Psi}_{i,n|n-1} - \hat{\mathbf{y}}_n^-\right)^T$$
$$\mathbf{K}_n = \mathbf{P}_{\tilde{x}_n\tilde{y}_n}\,\mathbf{P}_{\tilde{y}_n\tilde{y}_n}^{-1}$$
$$\hat{\mathbf{x}}_n = \hat{\mathbf{x}}_n^- + \mathbf{K}_n\,(\mathbf{Y}_n - \hat{\mathbf{y}}_n^-)$$
$$\mathbf{P}_n = \mathbf{P}_n^- - \mathbf{K}_n\,\mathbf{P}_{\tilde{y}_n\tilde{y}_n}\,\mathbf{K}_n^T$$

if convergence:

for each source:

$$\phi_l = \tan^{-1}\left(\frac{b_l}{a_l}\right)$$
$$\theta_l = \tan^{-1}\left(\frac{a_l}{c_l}\right)$$
$$\lambda_l = \frac{\cos\theta_l}{c_l}$$

break loop

the measurements. They are updated based on the difference between the predicted observations $\mathbf{y}_n^-$ and the actual measurements $\mathbf{Y}_n$. The predicted observations are evaluated as a weighted mean of the resultant of the measurement model after the sigma points are propagated through it. The complete algorithm used in prediction and updating steps are shown in Algorithm 2. The filter keeps going in iterations of selecting the sigma points, prediction and updating, till it converges to the true values. Finally, the carrier frequencies, azimuth angles and elevation angles are evaluated.

UKF tends to have a better performance than EKF, as UKF is accurate to the third order derivatives. Furthermore, UKF, unlike EKF, is a derivative-free filter. However, it requires calculating sigma points using Cholesky decomposition in every iteration. This leads UKF to have higher processing time.

V. RESULTS AND DISCUSSIONS

Numerical simulations of the proposed approaches are presented in this section. We first present the simulation model, and then we discuss the results. Finally, a comparison among our proposal and the proposals in [13] and [19] is presented.

A. SIMULATION MODEL

For simulations, each ULA on each axis has 150 elements ($N = 150$) with an inter-element spacing of one-fourth of the minimum wavelength. Twelve different source signals are impinging on the arrays. The source signals are traveling from different angles and are carried on different carrier frequencies. The normalized carrier frequencies of the source signals are {0.463, 0.217, 0.294, 0.716, 0.607, 0.861, 354, 0.119, 0.67, 0.294, 0.52, 0.4} respectively. The azimuth angles of the sources in degrees are {30, 47, 93, 52, 127, 173, 60, 205, 146, 26, 237, 100} and the elevation angles in degrees are {5, 84, 23, 37, 53, 127, 94, 151, 89, 163, 77, 41} respectively. The signal-to-noise ratio (SNR) is selected to be 5dB

The initial estimates in both EKF and UKF are set to values that are close to the mean value of the state variable. Thus, all elements in the initial estimate vector $\hat{\mathbf{x}}_o$ are set to 0.03. For simplicity, we assign all the elements to the same values, however they can randomly and differently be chosen around the mean value of $\mathbf{x}_s$. The initial covariance matrix $\mathbf{P}_0$ is also set to a proper value which prevents the filter from fully trust the estimates and ignoring the observations. Thus, we initialize it with its true value. Then, the filters are tuned carefully to guarantee the filter convergence. So, we properly set the matrices $\mathbf{R}$ and $\mathbf{P}_\upsilon$ in EKF and UKF respectively.

B. SIMULATION RESULTS

Under this scenario, Monte-Carlo simulations have been executed with both EKF and UKF for 500 snapshots. Both filters succeeded in detecting carrier frequency and 2D-DOA of all source signals. The root mean square error (RMSE) in the estimated parameters is shown in Figure 2a. Although EKF and UKF are sub-optimal estimators, they successfully detect the different sources with RMSE in all the estimated parameters close to 10^{-1}. The reason is that the estimated values are located in the same range and the initial estimates are set to the center of that range. These factors helped the filters to converge to the true values. However, both EKF and UKF

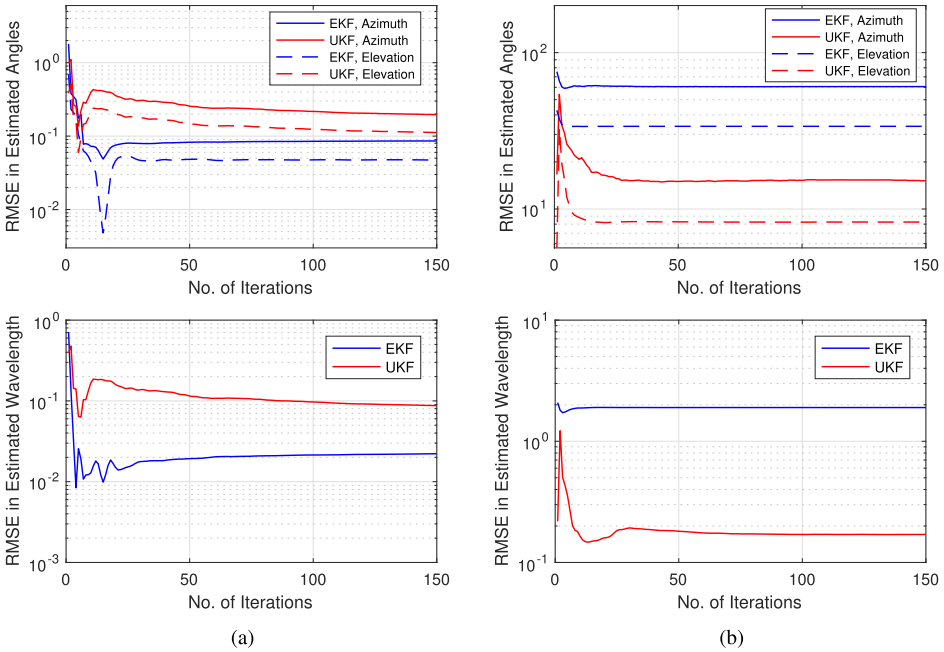

FIGURE 2. RMSE in the estimated azimuth, elevation and normalized wavelength at different initial estimates. (a) Initial estimate = 0.03. (b) Initial estimate = 0.7.

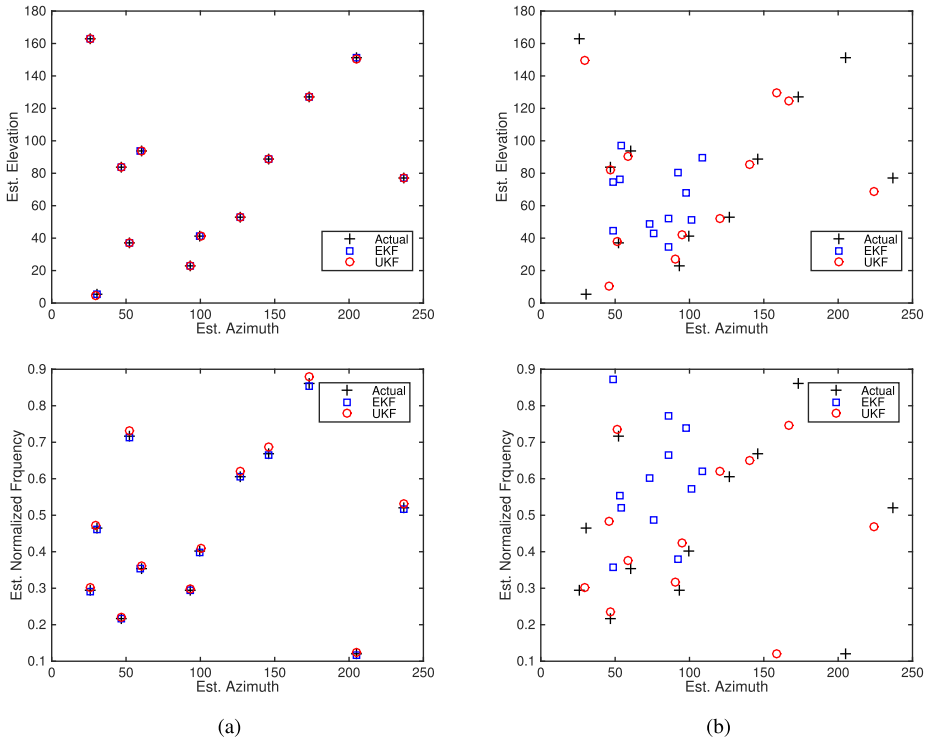

FIGURE 3. Estimated carrier frequencies and their corresponding 2D-DOA. (a) Initial estimate = 0.03. (b) Initial estimate = 0.7.

showed a degraded performance when the initial estimates were set to 0.7. In this case, RMSE deteriorated markedly as shown in Figure 2b. To explicitly declare those findings, the estimated carrier frequency and 2D-DOA in the two cases are shown in Figure 3. In Figure 3a, the estimated parameters are obviously close to the actual values when the initial estimate is 0.03. However, when the initial estimate was set to 0.7, EKF converged to erroneous values which are far apart from

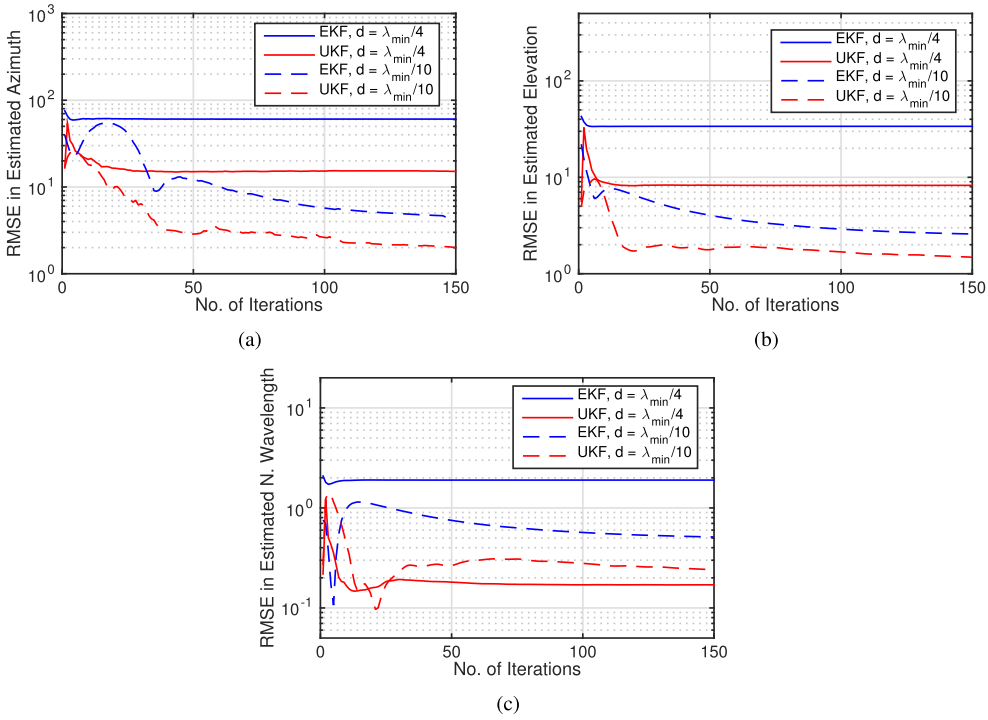

FIGURE 4. RMSE in the estimated azimuth, elevation and normalized wavelength with initial estimates of 0.7 and different inter-element spacing. (a) RMSE in Azimuth. (b) RMSE in Elevation. (c) RMSE in N. Wavelength.

the true values and UKF converged to the true values with massive errors as shown in Figure 3b. This proves that initial estimates play a crucial role in the filter convergence and may lead the filter to completely diverge if they are not set properly. Another thing can be found in Figure 2. When the initial estimate is 0.7, UKF outperforms EKF. That is expected, as UKF is accurate to the third derivative while EKF is accurate to the first derivative. However, EKF outperforms UKF when the initial estimate is 0.03. This indicates that the filter operates over a relatively linear model where the linearization error is massively reduced. This also reflects the vital role of initial estimates.

The inter-element spacing of the array can enhance the performance of EKF and UKF. As reducing the inter-element spacing expands the process model relating to the estimated parameters a_l, b_l and c_l. Expanding a nonlinear model can produce relatively linear characteristics over the region where those parameters are defined. This is proven by the improved performance accomplished by reducing the inter-element spacing. A new experiment has been executed with an initial estimate of 0.7 to show the effect of the inter-element spacing in a worse case. For different inter-element spacing values, simulations have been carried out and the results are shown in Figure 4. When the inter-element spacing is reduced to one-tenth of the minimum wavelength, the performance of both EKF and UKF is enhanced and the RMSE is reduced. Moreover, EKF performance starts to approach UKF performance and the gab between their performances is tremendously diminished. This indicates that the linearization error has been reduced and the process model tends to be relatively linear. Reducing the inter-element spacing, however, produces mutual coupling in the array elements.

Another experiment has been carried out to find out the effect of the number of source signals. The simulations have been repeated for 5, 12 and 24 source signals with inter-element spacing of $\lambda_{min}/10$ and initial estimate of 0.03. The filters were still able to detect all the carrier frequencies with their corresponding elevation and azimuth angles as shown in Figure 5. The filters can continue to detect a larger number of sources up to the degrees of freedom of two L-shaped uniform arrays. The degrees of freedom are limited to the number of array elements in one axis. Thus, the maximum number of source signals that can be detected with this system is 149. Since the detection of PUs is a blind estimation problem in CR, the CRs have no prior information about the number of existing sources. In this case, the filters are set to detect 149 different source signals and finally detect the actual number of the sources, as the remaining signals would be zero. As depicted in Figure 5, our approaches can detect azimuth angles up to 300°. As two L-shaped uniform arrays provide the ability to detect a range of azimuth angles of 360° and a range of elevation angles of 180°. In Figure 5c, There are many pairs that share the same frequency or the same elevation, but the two filters were able to distinguish between them since they differ in the other parameters.

From simulations, we found that EKF consumes time 20 times lower than the time consumed by UKF to detect 5 different sources. When the number of source signals

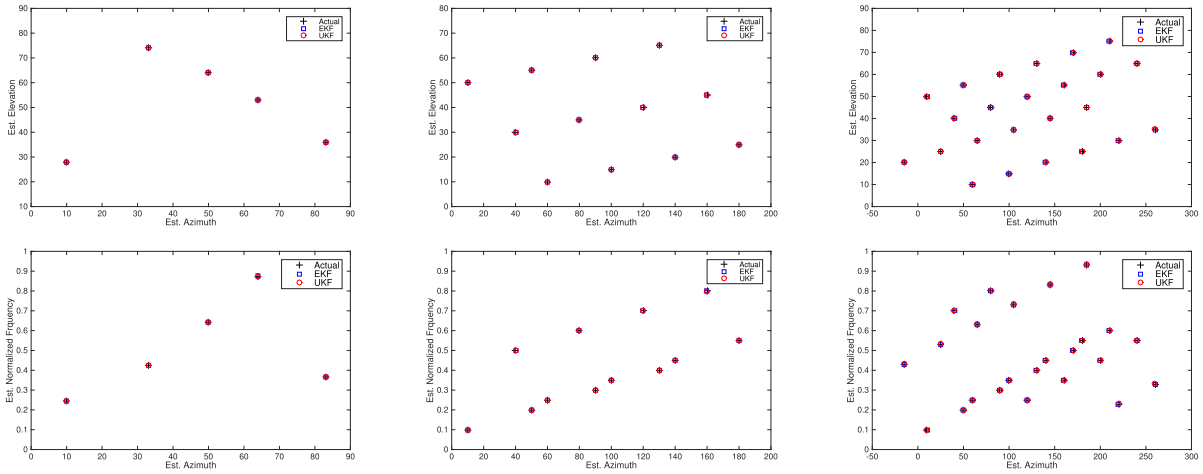

FIGURE 5. Estimated carrier frequencies and their corresponding 2D-DOA for different number of sources. (a) L = 5. (b) L = 12. (c) L = 24.

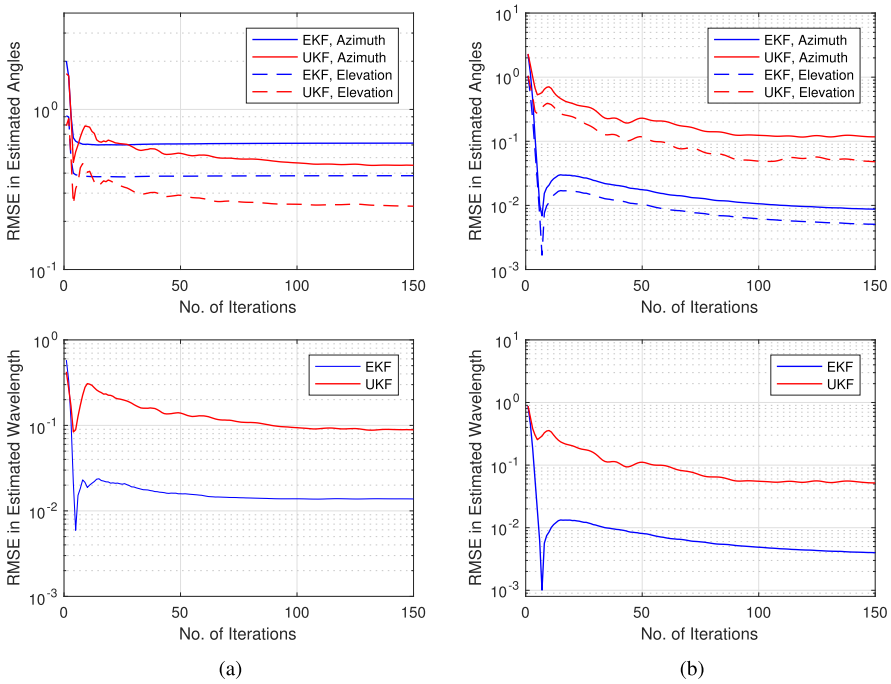

FIGURE 6. RMSE in the estimated carrier frequencies and their corresponding 2D-DOA at different SNRs. (a) SNR = 1dB. (b) SNR = 13dB.

is raised to 12, the ratio between the time consumed by UKF and EKF roughly becomes 40. Again, this ratio becomes around 70, when the number of sources becomes 24. Although UKF is a derivative-free, it consumes much time in selecting sigma points. Since the number of sigma points depends on the number of source signals, the time consumed by UKF to calculate and process these sigma points increases rapidly with the increase in the number of sources.

A further experiment has been carried out to examine our proposal at different levels of SNRs. Thus, we have repeated the simulations with an initial estimate of 0.03 and inter-element spacing of one-tenth of the minimum wavelength. The SNR level was set to 1dB and 13dB respectively, and RMSE in the estimated parameters was evaluated at each level. The results are gathered in Figure 6. At each SNR level, the filters should be tuned again to handle the new level of uncertainty in the measurements. The filter tuning is a trial-and-error process, where we keep on changing the matrix $\mathbf{R}$ till the filter converges. Therefore, the resultant RMSE follows both the SNR level and the quality of tuning as well. In overall, Figure 6 shows an improvement in the filter performance with the increase in SNR. EKF still follows the

same behavior as in Figure 3a and outperforms UKF because of selecting the initial estimate around zero and the small inter-element spacing.

C. COMPARATIVE STUDY

References [13] and [19] are considered for the sake of comparison. In [13], the authors have proposed a new architecture with a 2D nested array to implement sub-Nyquist sampling. The 2D nested array consists of two rectangular arrays: a sparse rectangular array and a dense one. To achieve sub-Nyquist rate, each element in the dense array is followed by a single ADC that samples the signals at sub-Nyquist rate. However, each element in the sparse array is followed by two paths: a direct path with an ADC and a delayed path with another ADC. Then, a proposed algorithm is executed to obtain the carrier frequency and a single DOA for each source. In [19], the authors have exploited a standard URA for detecting both the carrier frequency and the corresponding 2D-DOA of each source. Then, the authors have proposed adding a number of delay channels after a single array element of the employed URA. Each delay channel has been provided with an ADC. Then, the authors have exploited the spatial and time delays to detect the unknown parameters using ESPRIT algorithm. In contrast, our proposal does not rely on this large number of ADCs as the processing is executed spatially.

Table 1 shows the differences among our proposal, Kumar *et al.* [13], [19]. Kumar *et al.* [19] can detect a number of source signals higher than the number of array elements if the number of the employed delay channels exceeds 4. However, the simulations in [19] have proven that the higher the number of delay channels, the higher the performance would be accomplished. Thus, the number of delay channels would be twice or triple the number of array elements. In this context, the degrees of freedom of Kumar *et al.* [19] increase exponentially with the increase in the number of the employed array elements. Under these circumstances, it outperforms our proposal and Kumar *et al.* [13]. Although the latter has degrees of freedom that also increase exponentially, they rise at a slower rate than the degrees of freedom of Kumar *et al.* [19]. That is predictable since Kumar *et al.* [19], unlike the others, has no constraints on detecting a number of source signals higher than the number of the employed array elements. However, Kumar *et al.* [13] needed at least 5 array elements to start detecting source signals. Besides, it started to detect a number of source signals higher than the number of the employed array elements when the number of array elements exceeded 13. Our proposal, however, started to detect signals with 4 array elements, and its degrees of freedom increase linearly with the increase of the array elements. Besides, its degrees of freedom are restricted to one-third of the total number of the employed array elements. Overall, our proposal has the lowest degrees of freedom among the three methods as it does not rely on sparsity on any domain.

On the other hand, our proposal has employed a lower number of ADCs as there are no restrictions on the sampling rate. Since both Kumar *et al.* [13] and Kumar *et al.* [19] operate at sub-Nyquist rates to sample a wideband spectrum, their implementations require a large number of relaxed ADCs. The number of ADCs required for Kumar *et al.* [13] is around 1.5 times the number of array elements. Kumar *et al.* [19] required a number of ADCs equal to the total number of the employed array elements and delay channels together. As a result, the number of ADCs may be 3 or 4 times the number of array elements, which can be considered as the price that has been paid for the high degrees of freedoms. However, our proposal exploits the spatial domain instead of the temporal domain to get rid of the need to sample the signals at Nyquist rates, and hence it only requires a number of ADCs equal to the number of the employed array elements without any restrictions on the speed of the ADCs. So the number of ADCs required for our proposal is always lower than the number required by Kumar *et al.* [13] and Kumar *et al.* [19] for the same number of array elements.

Moreover, both our proposal and Kumar *et al.* [19] detect two angles for each source signal instead of a single angle

TABLE 1. Comparison among our proposed approaches, Kumar *et al.* [19] and Kumar *et al.* [13].

	Kumar *et al.* [19]	Kumar *et al.* [13]	KF-Based Proposed Approaches
Architecture	A URA with N elements and M delay channels	A 2D nested array with N elements	Two L-shaped uniform arrays with $3N-2$ elements
Degrees of Freedom	$\frac{NM}{4}$	$\left\lceil \frac{N}{4} \right\rceil^2 - 1$	$N-1$
Minimum Sampling Rate	$(N+M)B^*$	$\frac{(3N+1)B^*}{2}$	No restrictions
No. of ADCs employed	$N+M$	$\frac{(3N+1)}{2}$	$3N-2$
Estimated Parameters	2D-DOA Carrier Frequency	DOA Carrier Frequency	2D-DOA Carrier Frequency

* B denotes the bandwidth of band-limited source signals.

as in Kumar *et al.* [13]. This gives them another advantage as it increases the spatial capacity. As many CRs can share two parameters with PUs at the same time without interfering them as they differ in the third parameter.

VI. CONCLUSIONS

In this paper, EKF and UKF are proposed for the problem of estimating carrier frequencies and 2D-DOA of uncorrelated band-limited source signals. Exploiting two different angles in the space increases the spatial capacity of CR. The main challenge of wideband sensing is the need to high Nyquist rates and high hardware requirements. In order to decrease hardware complexity, KF is applied in the spatial domain where the incident signal on one array element is predicted from its version impinges on the previous array element. As a result, the proposed algorithm does not require complex hardware to perform Nyquist or sub-Nyquist rates. Since EKF and UKF are sub-optimal filters, they may converge to sub-optimal values or even diverge. To overcome this problem, the parameters to be estimated are scaled to the same range with small variance, and the filters should be properly initialized. Simulations have proven the vital effect of the initial estimates and inter-element spacing on the performance of the filters. The smaller the inter-element spacing, the higher the performance is. Since the proposal depends on two L-shaped uniform arrays, it has limited degrees of freedom restricted to the number of array elements. However, it has the availability to detect source signals from all directions in the space.

REFERENCES

[1] S. Haykin, "Cognitive radio: Brain-empowered wireless communications," *IEEE J. Sel. Areas Commun.*, vol. 23, no. 2, pp. 201–220, Feb. 2005.
[2] T. Yucek and H. Arslan, "A survey of spectrum sensing algorithms for cognitive radio applications," *IEEE Commun. Surveys Tuts.*, vol. 11, no. 1, pp. 116–130, 1st Quart., 2009.
[3] F. Salahdine, N. Kaabouch, and H. El Ghazi, "A survey on compressive sensing techniques for cognitive radio networks," *Phys. Commun.*, vol. 20, pp. 61–73, Sep. 2016. [Online]. Available: http://www.sciencedirect.com/science/article/pii/S1874490716300386
[4] A. A. Kumar, S. G. Razul, and C.-M. S. See, "An efficient sub-Nyquist receiver architecture for spectrum blind reconstruction and direction of arrival estimation," in *Proc. IEEE Int. Conf. Acoust., Speech Signal Process. (ICASSP)*, May 2014, pp. 6781–6785.
[5] A. A. Kumar, S. G. Razul, and C.-M. S. See, "Spectrum blind reconstruction and direction of arrival estimation at sub-Nyquist sampling rates with uniform linear array," in *Proc. IEEE Int. Conf. Digit. Signal Process. (DSP)*, Jul. 2015, pp. 670–674.
[6] R. Roy and T. Kailath, "Esprit-estimation of signal parameters via rotational invariance techniques," *IEEE Trans. Acoust., Speech, Signal Process.*, vol. 37, no. 7, pp. 984–995, Jul. 1989.
[7] R. O. Schmidt, "Multiple emitter location and signal parameter estimation," *IEEE Trans. Antennas Propag.*, vol. AP-34, no. 3, pp. 276–280, Mar. 1986.
[8] A. A. Kumar, S. G. Razul, and C.-M. S. See, "Spectrum blind reconstruction and direction of arrival estimation of multi-band signals at sub-Nyquist sampling rates," in *Multidimensional Systems and Signal Processing*. Springer, Sep. 2016, pp. 1–27, doi: 10.1007/s11045-016-0455-7.
[9] S. Stein, O. Yair, D. Cohen, and Y. C. Eldar, "Joint spectrum sensing and direction of arrival recovery from sub-Nyquist samples," in *Proc. IEEE 16th Int. Workshop Signal Process. Adv. Wireless Commun. (SPAWC)*, Jun. 2015, pp. 331–335.
[10] M. Mishali and Y. C. Eldar, "From theory to practice: Sub-Nyquist sampling of sparse wideband analog signals," *IEEE J. Sel. Topics Signal Process.*, vol. 4, no. 2, pp. 375–391, Apr. 2010.
[11] Z. Xiaofei, L. Jianfeng, and X. Lingyun, "Novel two-dimensional DOA estimation with L-shaped array," *EURASIP J. Adv. Signal Process.*, vol. 2011, p. 50, Dec. 2011.
[12] S. S. Ioushua, O. Yair, D. Cohen, and Y. C. Eldar, "CaSCADE: Compressed carrier and DOA estimation," *IEEE Trans. Signal Process.*, vol. 65, no. 10, pp. 2645–2658, May 2017.
[13] A. A. Kumar, S. G. Razul, and C. M. S. See, "Carrier frequency and direction of arrival estimation with nested sub-Nyquist sensor array receiver," in *Proc. 23rd Eur. Signal Process. Conf. (EUSIPCO)*, Aug. 2015, pp. 1167–1171.
[14] A. Lavrenko *et al.*, "Spatially resolved sub-Nyquist sensing of multiband signals with arbitrary antenna arrays," in *Proc. IEEE 17th Int. Workshop Signal Process. Adv. Wireless Commun. (SPAWC)*, Jul. 2016, pp. 1–5.
[15] D. D. Arianandа and G. Leus, "Compressive joint angular-frequency power spectrum estimation," in *Proc. 21st Eur. Signal Process. Conf. (EUSIPCO)*, Sep. 2013, pp. 1–5.
[16] C. Hui, W. Yongliang, and W. Zhiwen, "Frequency and 2-D angle estimation based on uniform circular array," in *Proc. IEEE Int. Symp. Phased Array Syst. Technol.*, Oct. 2003, pp. 547–552.
[17] X. Qi, L. Gan, P. Wei, and C. Ren, "Joint frequency and 2-D DOA estimation using pseudocovariance matrices," in *Proc. IEEE Int. Conf. Commun., Circuits Syst.*, Jul. 2009, pp. 398–401.
[18] R. J. Weber and Y. Huang, "A wideband circular array for frequency and 2D angle estimation," in *Proc. IEEE Aerosp. Conf.*, Mar. 2010, pp. 1–8.
[19] A. A. Kumar, M. G. Chandra, and P. Balamuralidhar, "Joint frequency and 2-D DOA recovery with sub-Nyquist difference space-time array," in *Proc. 25th Eur. Signal Process. Conf. (EUSIPCO)*, Sep. 2017, pp. 420–424.
[20] L.-T. Wan, L.-T. Liu, W.-J. Si, and Z.-X. Tian, "Joint estimation of 2D-DOA and frequency based on space-time matrix and conformal array," *Sci. World J.*, vol. 2013, 2013, Art. no. 463828.
[21] Y. Zou, H. Xie, L. Wan, and G. Han, "High accuracy frequency and 2D-DOAs estimation of conformal array based on PARAFAC," *J. Internet Technol.*, vol. 16, no. 1, pp. 107–119, 2015.
[22] L.-Y. Xu, X.-F. Zhang, Z.-Z. Xu, and M. Yu, "Joint 2D-DOA and frequency estimation for L-shaped array using iterative least squares method," *Int. J. Antennas Propag.*, vol. 2012, Sep. 2012, Art. no. 983092.
[23] G. Welch and G. Bishop, "An introduction to the Kalman filter," in *Proc. SIGGRAPH*, 2006, pp. 1–16.
[24] S. J. Julier and J. K. Uhlmann, "New extension of the Kalman filter to nonlinear systems," *Proc. SPIE*, vol. 3068, pp. 182–193, Apr. 1997.

SAMAR ELARABY received the B.Sc. degree in electronics and communication engineering from Port Said University, Egypt, in 2011, where she is currently pursuing the master's degree in electronics and communication engineering with the Faculty of Engineering. Her current research interests focus on cognitive radio, wireless communication, and signal processing.

HEBA Y. SOLIMAN received the B.Sc. degree in electrical communications and the M.Sc. degree in wireless communications from Suez Canal University in 1999 and 2004, respectively, and the Ph.D. degree in smart antenna systems from Port Said University in 2010. She is currently an Assistant Professor with the Electrical Engineering Department, Faculty of Engineering, Port Said University. Her research interests include adaptive antenna systems, MIMO systems, and cognitive radio.

HEBA M. ABDEL-ATTY received the Ph.D. degree in electronics and communications engineering from the Faculty of Engineering, Port Said University, Egypt, in 2012. She has been an Assistant Professor with the Electronics and Communications Engineering Department, Faculty of Engineering, Port Said University, since 2012. She is the Founder and the Counselor of the IEEE in Port-Said University Student Branch. Her current research interests are in wireless communication systems, mobile communication, multimedia processing, cognitive radio, security of wireless networks, and field programmable gate array applications.

MOHAMED A. MOHAMED received the Ph.D. degree in electronics and communications engineering from the Faculty of Engineering, Mansoura University, Egypt, in 2006. He was an Assistant Professor with the Electronics and Communications Engineering Department, where he has been an Associate Professor since 2012. He is currently the Executive Director of the Scientific Computing Center and a consultant for IT with Mansoura University. He has 130 publications in various international journals and conferences. His current research interests are in multimedia processing, wireless communication systems, and field programmable gate array applications. He received the Best Ph.D. Thesis from Mansoura University in 2007.